Antenna-Filter-Splitter Function Reconfigurable Microwave Passive Device Based on VO_2

Lei Sang, *Senior Member, IEEE*, Xiaoxiao Guo, Ji Xu, Xing Li, Mark Kraman, Yongfeng Mei, and Wen Huang, *Senior Member, IEEE*

***Abstract*—We designed and fabricated a three-in-one function reconfigurable microwave passive device, which can be functionally reconfigured to operate either as a radiating antenna, bandpass filter, or a two-way T-type power splitter. The device's function reconfigurability is enabled by locally sputtering vanadium dioxide (VO_2) phase transition thin films, which adjust the shape of conductor resonance patch and interconnect to electrically connect or isolate copper planar transmission lines and the patch on a sapphire substrate. Controlling the combination of the phases of four VO_2 thin-films interconnects effectively matches impedance and guides microwave signals, enabling the device's electromagnetic response to be reconfigured without reconstructing the physical structure. For different functions, the return loss and realized gain of patch antenna are 21 dB and −0.98 dBi at 4.75 GHz, respectively; the insertion loss of bandpass filter is 2.8 dB with bandwidth of 150 MHz (4.66–4.81 GHz); the dividing loss of power splitter is 5.0 dB at 4.7 GHz with power and phase imbalance within ±0.5 dB and ±7° from 4.4 to 5.0 GHz, respectively. Combining three devices in series enables more than 13 types of operation, which are suitable for different microwave systems.**

***Index Terms*—Function reconfigurable, microwave passive device, phase transition, reconfigurable passive device.**

I. Introduction

FOR numerous applications, including cube satellites, microrobotics, and wireless intelligence terminals, reusability is an important design feature that need to be considered. Characteristics of versatility, such as reconfigurability, programmability, and multifunctionality, are popular in the space of advanced highly integrated wireless communication circuits and systems because these design virtues are valuable to the alleviation of spectrum congestion and interference [1]–[4].

Impressive progress has been made on performance reconfigurable microwave planar passive devices, such as frequency [5], [6], radiation pattern [7], [8] or polarization reconfigurable antennas [9], [10] designed based on p-i-n switch, and variable capacitor or origami membrane technology [11], [12]. Among them, there is a relative lack of work on microwave devices with functional reconfigurability based on passive components whose operating mechanism is analogous to that of a field-programmable gate array.

Recently, a programmable antenna and filter two-in-one RF/microwave circuit based on p-i-n diode switches has been demonstrated [13]. In order to further improve functional reconfigurable microwave devices, we propose another feasible design methodology and demonstrate an antenna-filter-splitter three-in-one device with the following novelty. The switching of functions is enabled by the thermally controlled phase transition of vanadium dioxide (VO_2) thin-film segments [14], which act as current switch and microwave signal impedance matching for redistribution of electromagnetic (EM) field on demand. Compared to the diode or MEMS RF switch, the integration of VO_2 thin film is easy and fully compatible with planar semiconductor processing that enhances performance tolerance. The phase transition of VO_2 thin film can be regulated via off-chip uncontacted temperature controlling apparatus with no additional on-chip dc bias circuits needed, which reduces the design complexity and the associated parasitic effects.

II. Design Method of Function Reconfigurable Devices

Distinct from the design flow of traditional single function microwave devices, function reconfigurable microwave device design can be divided into three main steps: basic building block (BBB) design (acting as foundational, reusable circuits), individual branch elements (IBEs) design (acting as individual circuits), and comprehensive optimization. Among them, the BBB must be the most carefully designed, as it determines the center frequency and the way of EM coupling.

We chose microwave passive device with three representative functionalities to illustrate the design process, which are those of an antenna, filter, and power splitter. For simplicity, only the most important figures-of-merit of each functionality are considered. Fig. 1 shows the general design flow of the function reconfigurable microwave passive devices, and the design details of BBB and IBE are illustrated as follows.

A. Determine BBB Architecture

By considering patch structure is frequently used in antenna, filter, and power splitter design, a Cu patch embedding VO_2 thin film in the trench and connecting another three smaller

Manuscript received June 22, 2020; accepted July 22, 2020. Date of publication July 28, 2020; date of current version October 6, 2020. This work was supported in part by the National Natural Science Foundation of China under Grant 61974038 and in part by the Fundamental Research Funds for the Central Universities of China under Grant JZ2020HGTB0037 and Grant JZ2020HGPB0116. *(Corresponding author: Wen Huang.)*

Lei Sang, Xiaoxiao Guo, Ji Xu, and Wen Huang are with the School of Microelectronics, Intelligent Interconnected Systems Laboratory of Anhui Province, Hefei University of Technology, Hefei 230601, China (e-mail: sanglei2008@126.com; 2051133176@qq.com; 3099196979@qq.com; huangw@hfut.edu.cn).

Xing Li and Yongfeng Mei are with the Department of Materials Science, Fudan University, Shanghai 200433, China (e-mail: usst_lx@126.com; yfm@fudan.edu.cn).

Mark Kraman is with the Department of Electrical and Computer Science, University of Illinois at Urbana-Champaign, Urbana, IL 610801 USA (e-mail: mkraman2@illinois.edu).

Digital Object Identifier 10.1109/LAWP.2020.3012192

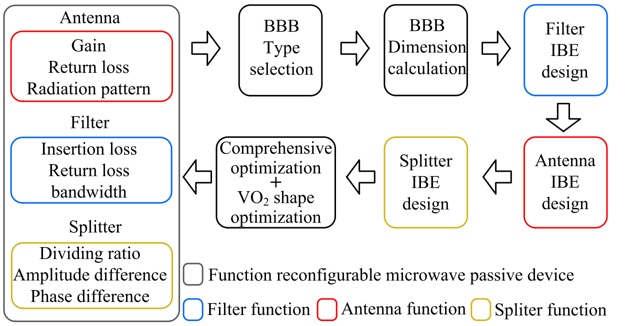

Fig. 1. General design flow of the demonstrative function reconfigurable microwave passive device based on VO_2 phase transition material.

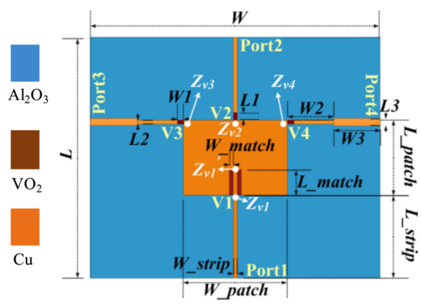

Fig. 2. Shape and critical dimensional parameters of the function reconfigurable device and the location of the VO_2 thin-film segments.

VO_2 thin films on the edge is chosen as the BBB, as shown in Fig. 2. As a phase transition material, the electrical conductivity of VO_2 thin film is able to be changed by several orders of magnitudes switching between resistive and conductive states at room temperature. Therefore, to realize the specific function, VO_2 thin film must be able to switch and direct the current flow to desired IBEs, and, most importantly, be able to fulfill the impedance matching of microwave signal according to the requirement of different functions. VO_2 thin film on location labeled by V_1 performs as impedance matching, while others on location labeled by V_2, V_3, and V_4 could be considered as switches [15], [16]. An operating frequency of 4.75 GHz was set as a global requirement for all EM functionalities due to its important placement in the 5G bands.

B. Determine BBB Dimension

For antenna operation, to accommodate a working frequency of 4.75 GHz at dominant mode (TM_{01}), the length of the BBB (*L_patch*) can be calculated to be 9.3 mm [17]. Then, it is well known that the design of rectangular patch filters is based on even/odd mode (TM_{01}/TM_{10}) analysis methods and coupling matrix *M*, which produce the physical dimensions of the BBB according to the desired performance merits such as the central frequency (f_c), frequency bandwidth (FBW), and insertion loss (IL) [18]. For simplicity, based on the basic first-order filter prototype, the known length of the BBB (*L_patch*) and the target performance merits of $f_c = 4.75$ GHz, FBW $= 5\%$, and IL $=$ 1 dB, the *M* matrix is solved as shown in the following equation and the width (*W_patch*) of BBB is calculated to be 13 mm:

$$[M] = \begin{bmatrix} 0 & 0.448 & 1.496 & 0 \\ 0.448 & 9.135 & 0 & 0.448 \\ 1.496 & 0 & -1.98 & -1.496 \\ 0 & 0.448 & -1.496 & 0 \end{bmatrix}. \tag{1}$$

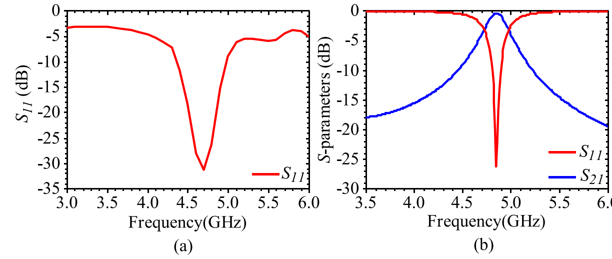

Fig. 3. Simulated performance of the designed device. (a) S_{11} versus frequency of the antenna functionality. (b) S_{11} and S_{21} versus frequency of the filter functionality.

C. Determine Filter IBE Dimension

When acting as a bandpass filter, the phase-transitioned conductive VO_2 thin films on locations V_1 and V_2 in the BBB compensate for the trench to generate the TM_{01} mode and conduct the current flow out, respectively, while others remain phase untransitioned. If better performance is desired, the VO_2 thin film can be used to mimic corner-cutting effects on the BBB to generate transmission zeroes 8 for improved selectivity.

Once the dimension of BBB is determined, under filter operation, the input impedances Z_{V1} and Z_{V2} can be calculated to be $42.7 + 2.1j\ \Omega$ and $41.3 + 2.3j\ \Omega$, according to resonant cavity theory by using equivalent voltage and current based on electric field distribution mode [19], respectively. Although the spots of V_1 and V_2 are symmetric, the discrepancy of the input impedance at the two spots is attributed to the lower conductivity of VO_2 at V_1 spot after phase transition compared to that of Cu thin film. Then, to match between the real part of the impedance Z_{V1} and Z_{V2} at the patch connection points and the 50 Ω standard input and output ports in narrow frequency band, quarter-wave feedlines with the length $L_{\_\text{strip}}$ of 10.35 mm and calculated width $W_{\_\text{strip}}$ of 0.52 and 0.56 mm were chosen.

D. Determine Antenna IBE Dimension

When acting as a patch antenna, the VO_2 thin films on locations V_1 and V_2 become untransitioned to form the trench to do impedance matching. By knowing the dimension of the filter IBE microstrip transmission line, the physical length L_{match} and width W_{match} of the trench window can be calculated by the equations developed in [18] to compensate for the imaginary part of Z_{V1}. Actually, the access point of input signal to BBB moves from Z_{v1} to Z'_{v1}, as shown in Fig. 2, and the impedance on the spot Z'_{v1} is calculated to be 50.6 Ω, which results in better S_{11} of the antenna function than that of the filter function.

With all the dimensions of antenna and filter determined, the antenna gain can be calculated as 1.1 dBi at 4.75 GHz. The *S*-parameters of the two functions are shown in Fig. 3. As the coupling coefficient is small, the second pole is far away from the TM_{01} renounce frequency point.

E. Determine Power Splitter IBE Dimension

After the design of antenna and filter, the dimension of the BBB and corresponding IBEs is actually determined. Therefore, the design of power splitter is to choose the right spots V_3 and V_4 of VO_2 thin film and the dimension of the power splitter IBEs. When acting as a power splitter, the phase-transitioned conductive VO_2 thin films on locations V_1, V_3, and V_4 conduct the current flow in and out, respectively, while V_2 remains phase

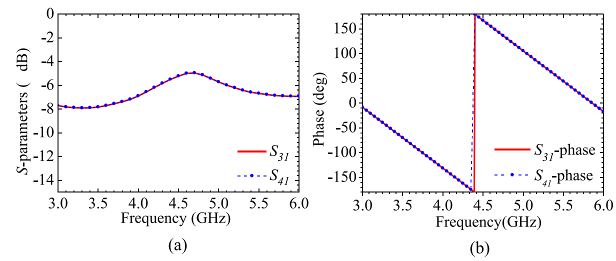

Fig. 4. Simulated power transmission and the phase delay of the splitter functionality. (a) The simulated power transmission loss of the T-type power splitter. (b) The phase delay of the T-type power splitter.

TABLE I
PHYSICAL DIMENSIONS OF THE DEMONSTRATIVE FUNCTION RECONFIGURABLE MICROWAVE PASSIVE DEVICE (UNITS: MILLIMETERS)

L	W	L_{patch}	W_{patch}	L_{strip}	L_2	L_3
30	36.2	9.3	13	10.35	0.5	0.56
L_1	W_1	W_2	L_{match}	W_{match}	W_{stri}	W_3
0.75	0.35	11.6	3.2	0.5	0.52	11

untransitioned. As shown in Fig. 2, compared to all the other spots around BBB, the spots of V_3 and V_4 are chosen at the upper corners of the BBB due to their input impedances Z_{V3} and Z_{V4} of the BBB have the largest value of 51.3 + 1.7j Ω, which are easier to do the impedance matching to 50 Ω. Two-step impedance transforming signal outlines were used, and the dimension can be determined based on the real part of the input impedance Z_{V3} and Z_{V4}. The power loss and the phase delay from 4.5 to 6 GHz then can be simulated and shown in Fig. 4.

F. Comprehensive Optimization

Even for the simplified demonstrative device, the design of different EM functionalities is not independent, and global consideration to co-optimize different operating modes is imperative. The decision of the physical size and access points of the VO_2 units will affect every functionality. Once the initial physical dimension is determined, a commercial finite element method analyzer such as high-frequency structure simulator (HFSS) is used for determining the size of VO_2 segments.

The width of VO_2 segments is equal to that of the contacted IBE lines, and the length of VO_2 segments is optimized to compromise between the EM coupling and IL between BBB and IBE before and after the VO_2 phase transition resulting in the length of 0.35, 0.35, and 0.75 mm for VO_2 segments on locations V_2, V_3, and V_4, respectively. Table I summarizes the physical dimensions of the demonstrative function reconfigurable microwave passive device. Table II summarizes three different modes of operation and their corresponding simulated current layouts.

III. PROCESS AND ELECTRICAL PROPERTIES OF THE VO_2

In this letter, a 2″ sapphire wafer with permittivity of 11.5 and thickness of 500 μm was used as the substrate, and the VO_2 thin film was deposited by direct-current magnetron sputtering with a high-purity vanadium metal target [20]. The growth pressure, Ar/O_2 gas flow, dc power, and temperature were 11.46 mTorr, 60/40 sccm, 200 W, and 580 °C respectively. The dc electrical conductivity and ac *S*-parameters were measured to vary over three orders of magnitude from 3×10^3 to 3.3×10^6 S/m

TABLE II
MODE FUNCTIONS OF THE FUNCTION RECONFIGURABLE MICROWAVE DEVICE

VO_2 unit phase combination*	V_1: M	V_2: M	V_1: T	V_2: T	V_1: T	V_2: M
	V_3: M	V_4: M	V_3: M	V_4: M	V_3: T	V_4: T
Corresponding current distribution at operating frequency at 4.75 GHz†	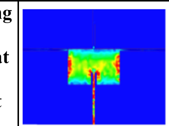		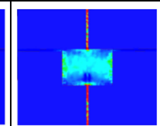		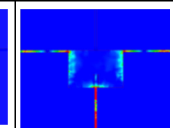	
Functionalities	Mode 1: Patch antenna		Mode 2: Bandpass Filter		Mode 3: Power splitter	

Top view of the device is shown. *Symbols M and T represent the monoclinic phase and tetragonal phase, respectively. †Color bar: J_{surf} (A/m) with 1 W input.

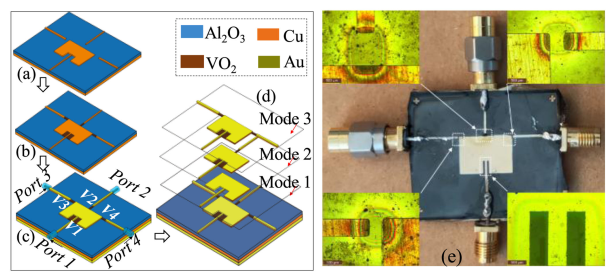

Fig. 5. Left image is the fabrication processing flow and the layout design of a multifunctional VO_2-based microwave passive device. The right optical image. (a) The step of Cu evaporation process. (b) The step of VO_2 evaporation process. (c) The step of Au evaporation process. (d) The mask correspond to each function. (e) Top view of the demonstrative function reconfigurable passive device utilizing VO_2 phase transition thin films on a sapphire substrate.

and average IL of ∼ 0.7 dB/mm 2–6 GHz after the phase transitions at 60 °C, respectively. Considering complementary metal-oxide-semiconductor (CMOS) processing compatibility, Cu is used as the primary conductive material, deposited by E-beam evaporation. As shown in Fig. 5(a), the backside of the sapphire substrate is fully covered by a Cu layer, and, on the front side, a Cu layer is patterned to form the BBB of the device and the specific element. VO_2 thin films with a thickness of 0.5 μm are then sputtered locally onto the sapphire substrate, as shown in Fig. 5(b) (a shadow mask is designed and used to cover the top side of the device during sputtering). To achieve a high-quality electrical connection between the subminiature version A (SMA) connectors and the microstrip transmission lines, a gold (Au) thin film with a thickness of 0.3 μm is deposited by E-beam evaporation to fully cover the surface of the Cu layer on both sides of the device, as shown in Fig. 5(c) (another shadow mask is used to cover the top side during sputtering). The schematic view of the functional layout under different operating modes is shown in Fig. 5(d) by local control of the phase transition of the VO_2.

IV. MEASUREMENT AND RESULT ANALYSIS

As shown in Fig. 5(e), four deposited VO_2 interconnects as observed under an optical microscope are shown in the corners. To locally control the phase of the VO_2 thin-film segments, an expanded polystyrene flat substrate with electric resistance wires superincumbent VO_2 segments was used (note that antenna function does not require any phase transition of VO_2). The temperature of the area undergoing heat treatment was monitored by infrared thermometer, ensuring that the phase transition of the VO_2 thin films would be triggered on demand. As the relative

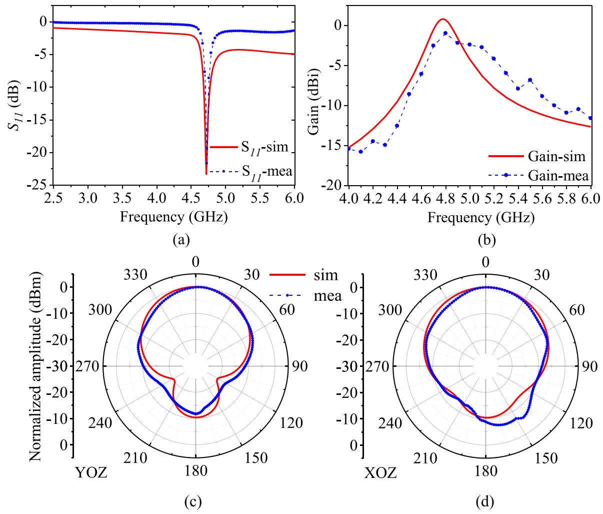

Fig. 6. Comparison between the simulated and the measured performance of the antenna functionality. (a)–(d) S_{11}, the gain, and radiation pattern.

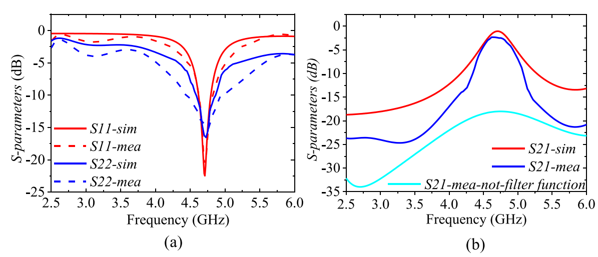

Fig. 7. Comparison between the simulated and the measured performance of the filter functionality. (a) S_{11} and S_{22} of the in/out port. (b) S_{21}.

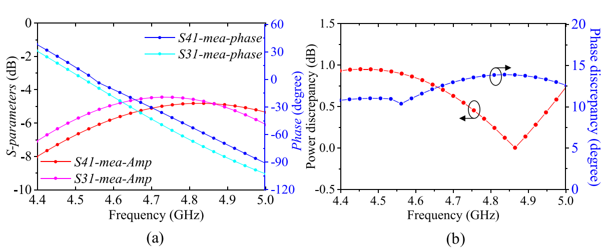

Fig. 8. Comparison between the simulated and measured performances of the splitter functionality. (a) Dividing amplitude and the phase delay. (b) Discrepancy of S_{31} and S_{41} in the designed working frequency band.

dielectric constant of expanded polystyrene is $\sim$1.2 and electric resistance wires noncontacting to the device are carefully wired, the parasitic effects introduced by heating setup is negligible. Comparisons between the simulated and measured performance metrics of each EM function of the sample are shown in Figs. 6 –8. As shown in Fig. 6(a)–(d), under antenna function mode, the measured antenna gain is more than -1 dBi with the S_{11} corresponding as shown, lower than -20 dB at 4.75 GHz. By defining the top view plane in Fig. 6 is the *xoy* plane, at this operating point, the 3 dB lobe width is greater than 55° and 48° on the *yoz* plane and *xoz* plane, respectively. For narrow bandpass filter mode operation, shown in Fig. 7(a) and (b), the IL is smaller than 2.8 dB and the out-of-band suppression is more than 12 dB 500 MHz away from the center frequency point. For the splitter function mode, the IL and phase delay of the T-power-splitter

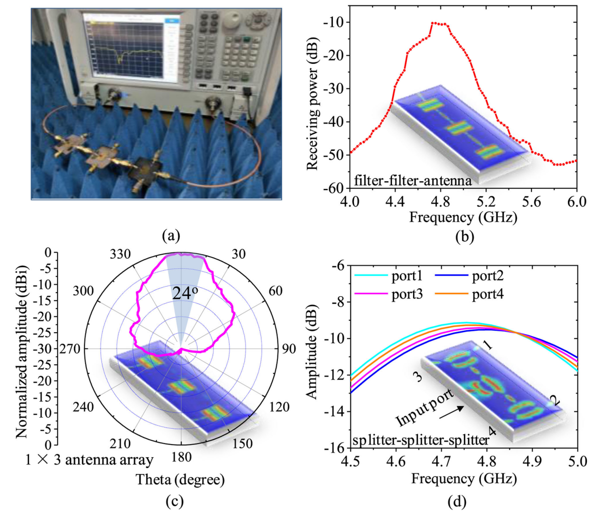

Fig. 9. Measured performance and simulated electric field distribution of three different combination modes. (a) The cascade connection of the three devices. (b) The frequency spectrum characteristic of the operation mode of antenna-filter-filter. (c) The pattern of the operation mode of 1×3 antenna array. (d) The transmission loss of the operation mode of three splitters.

from port 1 to port 3/port 4 are shown in Fig. 8(a) and (b). The division loss S_{31}/ S_{41} is $\sim$4.7/5.2 dB at 4.7 GHz. From 4.4 to 5.0 GHz, the imbalance of the output power is within $\pm$0.5 dB and the imbalance of phase is within $\pm 7°$.

The discrepancy between simulation and measurement is mainly due to mask alignment and the quality of the manually soldered SMA connectors. Compared to high-conductivity metal, such as Cu, the lower conductivity of phase-changed VO_2 thin film introduces more ohmic loss. Even so, each EM function meets their basic requirements, meaning that the intended independent operating modes are able to be realized through the same device.

For one of the application demonstrations, as shown in Fig. 9(a), three identical three-in-one devices in series form a reconfigurable passive network, which increases the number of potential network functions to 13 in this case. As shown in Fig. 9(b) the combination of the antenna–filter–filter configuration has a narrow receiving power spectrum which is suitable for anti-interference systems. The 1×3 array patch antenna is composed of three series devices with a narrow radiation pattern, as shown in Fig. 9(c). The 1:4 power divider is composed of three series function reconfigurable devices configured as splitters. Fig. 9(d) shows that the microwave signal goes through the input port of the middle device and be divided into the four output ports of the side devices with small amplitude imbalance.

V. Conclusion

A phase transition enabled EM function reconfigurable microwave passive device is demonstrated by utilizing sputtered VO_2 thin-film segments on a sapphire substrate. EM functions, such as antenna radiation, bandpass signal filtering, and two-way power division, are obtained through the physical structure. A potential reconfiguration mechanism for RF/microwave front-end systems is discussed. Compared to the conventional understanding of reconfigurability, the function reconfigurable concept proposed in this letter shows a clear alternative to address the ever-present and increasingly urgent need to realize supercompact footprint metrics while concurrently improving the performance of microwave electronic devices and systems.

REFERENCES

[1] L H. Trinh, F. Ferrero, L. Lizzi, R. Staraj, and J. Ribero, “Reconfigurable antenna for future spectrum reallocations in 5G communications,” *IEEE Antennas Wireless Propag. Lett.*, vol. 15, pp. 1297–1300, 2016.

[2] S. J. Chen, D. C. Ranasinghe, and C. Fumeaux, “A robust snap-on button solution for reconfigurable wearable textile antennas,” *IEEE Trans. Antennas Propag.*, vol. 66, no. 9, pp. 4541–4551, Sep. 2018.

[3] S. M. Saeed, C. A. Balanis, C. R. Birtcher, A. C. Durgun, and H. N. Shaman, “Wearable flexible reconfigurable antenna integrated with artificial magnetic conductor,” *IEEE Antennas Wireless Propag. Lett.*, vol. 16, pp. 2396–2399, 2017.

[4] L. Sun, Z. Zhang, F. Zhang, and A. Chen, “L/S multiband frequency reconfigurable antenna for satellite applications,” *IEEE Antennas Wireless Propag. Lett.*, vol. 18, no. 12, pp. 2617–2621, Dec. 2019.

[5] S. Y. Sun, W. Jiang, S. Gong, and T. Hong, “Reconfigurable linear-to-linear polarization conversion metasurface based on PIN diodes,” *IEEE Antennas Wireless Propag. Lett.*, vol. 17, no. 9, pp. 1722–1726, Sep. 2018.

[6] S. Lee, S. I. H. Shah, H. L. Lee, and S. Lim, “Frequency-reconfigurable antenna inspired by origami flasher,” *IEEE Antennas Wireless Propag. Lett.*, vol. 18, no. 8, pp. 1691–1695, Aug. 2019.

[7] C. M. Lee and C. W. Jung, “Radiation-pattern-reconfigurable antenna using monopole-loop for fitbit flex wristband,” *IEEE Antennas Wireless Propag. Lett.*, vol. 14, pp. 269–272, 2015.

[8] J. Li, M. He, C. Wu, and C. Zhang, “Radiation-pattern-reconfigurable graphene leaky-wave antenna at terahertz band based on dielectric grating structure,” *IEEE Antennas Wireless Propag. Lett.*, vol. 16, pp. 1771–1775, 2017.

[9] L. Tan, R. Wu, and Y. Poo, “Magnetically reconfigurable SIW antenna with tunable frequencies and polarizations,” *IEEE Trans. Antennas Propag.*, vol. 63, no. 6, pp. 2772–2776, Jun. 2015.

[10] N. Nguyen-Trong, A. Piotrowski, L. Hall, and C. Fumeaux, “A frequency- and polarization-reconfigurable circular cavity antenna,” *IEEE Antennas Wireless Propag. Lett.*, vol. 16, pp. 999–1002, 2017.

[11] M. Bouslama, M. Traii, T. A. Denidni, and A. Gharsallah, “Beam switching antenna with a new reconfigurable frequency selective surface,” *IEEE Antennas Wireless Propag. Lett.*, vol. 15, pp. 1159–1162, 2016.

[12] S. M. Mahmood and T. A. Denidni, “Pattern-reconfigurable antenna using a switchable frequency selective surface with improved bandwidth,” *IEEE Antennas Wireless Propag. Lett.*, vol. 15, pp. 1148–1151, 2016.

[13] A. L. Borja, Y. Kabiri, A. Belenguer, and J. R. Kelly, “Programmable multifunctional RF/microwave circuit for antenna and filter operation,” *IEEE Trans Antennas Propag.*, vol. 66, no. 8, pp. 3865–3876, Aug. 2018.

[14] S. D. Ha, Y. Zhou, C. J. Fisher, S. Ramanathan, and J. P. Treadway, “Electrical switching dynamics and broadband microwave characteristics of VO_2 radio frequency devices,” *J. Appl. Phys.*, vol. 113, no. 18, 2013, Art. no. 184501.

[15] N. Émond, A. Hendaoui, S. Delprat, M. Chaker, and K. Wu, “Theoretical and experimental investigation of thermo-tunable metal–insulator–vanadium dioxide coplanar waveguide structure,” *IEEE Trans. Microw. Theory Techn.*, vol. 65, no. 5, pp. 1443–1455, May 2017.

[16] K. C. Pan, W. S. Wang, E. S. Shin, F. Kelvin, and S. Guru, “Vanadium oxide thin-film variable resistor-based RF switches,” *IEEE Trans. Electron. Devices*, vol. 62, no. 9, pp. 2959–2965, Sep. 2015.

[17] J. R. James, P. S. Hall, and C. Wood, *Microstrip Antenna Theory and Design*. London, U.K.: Peregrinus, 1981.

[18] D. M. Pozar, *Microwave Engineering*, 4th ed. Hoboken, NJ, USA: Wiley, 2006.

[19] K. Dutta, D. Guha, and C. Kumar, “Theory of controlled aperture field for advanced superstrate design of a resonance cavity antenna with improved radiations properties,” *IEEE Trans. Antennas Propag.*, vol. 65, no. 3, pp. 1399–1403, Mar. 2017.

[20] L. Otto *et al.*, “Antenna-assisted picosecond control of nanoscale phase transition in vanadium dioxide,” *Nature Mater.*, vol. 5, 2016, Art. no. 16173.